PROTEINS
STRUCTURE ■ FUNCTION ■ BIOINFORMATICS

Thermodynamics of Aβ_{16-21} dissociation from a fibril: Enthalpy, entropy, and volumetric properties

Srinivasa Rao Jampani, Farbod Mahmoudinobar, Zhaoqian Su, and Cristiano L. Dias*

Department of Physics, New Jersey Institute of Technology, Newark, New Jersey 07102-1982

ABSTRACT

Here, we provide insights into the thermodynamic properties of Aβ_{16-21} dissociation from an amyloid fibril using all-atom molecular dynamics simulations in explicit water. An umbrella sampling protocol is used to compute potentials of mean force (PMF) as a function of the distance ξ between centers-of-mass of the Aβ_{16-21} peptide and the preformed fibril at nine temperatures. Changes in the enthalpy and the entropic energy are determined from the temperature dependence of these PMF(s) and the average volume of the simulation box is computed as a function of ξ. We find that the PMF at 310 K is dominated by enthalpy while the entropic energy does not change significantly during dissociation. The volume of the system decreases during dissociation. Moreover, the magnitude of this volume change also decreases with increasing temperature. By defining dock and lock states using the solvent accessible surface area (SASA), we find that the behavior of the electrostatic energy is different in these two states. It increases (unfavorable) and decreases (favorable) during dissociation in lock and dock states, respectively, while the energy due to Lennard-Jones interactions increases continuously in these states. Our simulations also highlight the importance of hydrophobic interactions in accounting for the stability of Aβ_{16-21}.

Proteins 2015; 83:1963–1972.

Key words: fibril; proteins; thermodynamics; entropy; enthalpy; heat capacity; thermal expansion; lock-dock states.

INTRODUCTION

Proteins are the workhorse of the living cell actualizing the information blueprinted in the DNA. They become inactive when prevented from folding into the native state and, under certain conditions, proteins aggregate into cross-β structures leading to fibrils.[1] The latter has been related to the end product of degenerative diseases like Alzheimer's and Parkinson's.[2,3] Moreover, fibrils exhibit superior mechanical strength, high aspect ratio, and resistant to denaturants.[4,5] Therefore, biological functions of proteins that are naturally encoded to form fibrils can involve structural support and protection against environment hazards. For examples, proteins in silkmoth eggshells form fibril-like structures that serve to protect the developing embryo.[6] Due to their importance, cross-β structures have been subjected to intensive scientific scrutiny.[7] However, it is still not clear what are the main molecular forces driving the formation of these structures and how they differ from the ones driving proteins into their native state. Determining these forces is of fundamental importance to understand the pathology of diseases and to design new fibril-like materials with tailored properties. This is a focus of the present work.

Thermodynamics provides a quantitative framework to study the stability and the forces driving conformational changes in proteins.[8] For example, at ambient conditions folding of single domain globular proteins is characterized by a favorable change in enthalpy ($\Delta H < 0$), an unfavorable change in the entropic energy ($-T\Delta S > 0$), and a negative change in the heat capacity ($\Delta C_p < 0$).[9–11] The magnitude of the change in heat capacity increases with the size of the protein[12] and it can be ascribed to nonpolar residues that are initially exposed to water and become buried in the dry core of the protein during folding.[13,14] The unfavorable entropic energy of folding has been related to reduced freedom of the backbone and side

Grant sponsor: NJIT.
Institution where the work was performed: New Jersey Institute of Technology, Department of Physics, 07102-1982, Newark, New Jersey
*Correspondence to: Cristiano L. Dias; Department of Physics, New Jersey Institute of Technology, Newark, New Jersey, 07102-1982. E-mail: cld@njit.edu
Received 17 April 2015; Revised 22 July 2015; Accepted 2 August 2015
Published online 12 August 2015 in Wiley Online Library (wileyonlinelibrary.com). DOI: 10.1002/prot.24875

chains (conformational entropy) in the folded state while the favorable enthalpy is due to the formation of native contacts. For many single domain globular proteins the magnitude of the enthalpy and entropic energy are of the same order ($\sim$100$-$200 kJ/mol)[15,16] accounting for a small free-energy difference $\Delta G \sim 30$ kJ mol^{-1} between native and unfolded states.[10,11]

Thermodynamic properties of fibril melting have been studied using differential scanning calorimetry whereby the heat capacity is measured at different temperatures.[17–20] In these experiments, peptides dissociate cooperatively and irreversibly from the fibril at the melting temperature. Irreversibility precludes the use of quantitative analyses to compute free energy differences (e.g., $-T\Delta S$, and ΔG) and as a result the thermodynamics of fibrillization remains largely an open question. Furthermore, fibrillization is not an all-in-one reaction similar to fibril melting. It emerges from a two step process in which peptides nucleate into small oligomeric units followed by growth into ordered cross-β structures.[21–25] The growth process proceeds through monomer addition[26–28] which involves two main steps described by a dock-lock mechanism.[29–33] In the first step, the peptide assumes mostly coil structures[34] while it docks into the fibril decreasing the overall solvent accessible surface area. This step is dominated by interactions between side chains of the peptide and the fibril and it is sequence-specific. In the second step the peptide locks into the fibril via non-specific hydrogen bonds between the backbone of the peptide and the fibril.[34,35] Estimates have shown that the slow formation time of the lock phase determines the rate of monomer addition.[29,36]

The emergence of fibrils as a nucleation and growth process appears to be a general feature of amyloid peptides that is independent of the amino acid sequences. However, the dynamics and stabilization mechanism of fibrils were reported to be dependent on the amino acid sequence. For example, the stability of polar sequences (Sub35, GNNQQNY) is enhanced by hydrogen bonds between side chains and the backbone forming a steric zipper not present in nonpolar sequences (Aβ_{16-22}, KLVFFAE).[36] Additional insight into how the amino acid sequence of peptides affect fibrils were obtained by computational studies of β-sheet stacking into a protofilament. In the case of β-sheets made from Aβ_{16-22} peptides, a subtle interplay was shown between an assembly driven by specific interactions between residues and one mediated by water. The latter suggests that dewetting could be a driving mechanism of β-sheet assembly.[37] In contrast, an ordered one-dimensional water wire was reported to stabilize β-sheets in the assembly of a protofilament made from Sup35 peptides.[38] Thus, water plays a different role in the assembly of polar and non-polar β-sheet which was estimated to cause a difference in the assembly time by a factor of 1000.[38,39]

While the cooperative dissociation of peptides from a fibril melting at high temperature is irreversible, fibril growth through monomer addition is expected to be reversible. Evidence of the latter was obtained by studying strongly seeded solutions in which fragmentation and nucleation of fibrils was negligible.[40] In these studies, amyloid fibrils were reported to grow to a reversible equilibrium position exhibiting a characteristic equilibrium constant and an associated free-energy of growth.[41] Furthermore, by measuring these free-energies for two Aβ peptides differing in sequence at one position it was possible to estimate contributions of specific amino acids to fibril growth.[42]

Despite these studies, the energetic terms characterizing lock, dock, and monomeric states remain largely unclear as well as thermodynamical quantities required to describe the stability of fibrils, for example, ΔH, $-T\Delta S$. The main goal of this manuscript is to compute these quantities for fibrils made of Aβ_{16-21} peptides and provide insights into their molecular basis through all-atom molecular dynamics simulations using explicit water models. To that purpose we use an umbrella sampling protocol to compute potentials of mean force (PMF) of peptide dissociation from a preformed protofibril at different temperatures.[43] ΔH, and $-T\Delta S$ are derived from the temperature dependence of these PMF(s). We find that the PMF at 310 K is dominated by enthalpy while the entropic energy does not change significantly during dissociation. The volume of the system decreases during dissociation. Moreover, the magnitude of this volume change also decreases with increasing temperature. Dock and lock states are defined based on the solvent accessible surface area (SASA). We observe that the behavior of the electrostatic energy is different in these two states. It increases and decreases during dissociation in lock and dock states, respectively, while the energy due to Lennard-Jones interactions increases continuously in these states. Our simulations also highlight the importance of hydrophobic interactions in accounting for the stability of Aβ_{16-21}.

METHODOLOGY

The initial fibril conformation of our simulations is based on the cross-β structure for Aβ_{16-21} (KLVFFA) that was resolved experimentally using ss-NMR (PDB ID: 3OW9).[44] Twelve peptides have been resolved in the experimental structure. Each peptide assumes a β-strand conformation that is arranged to form two anti-parallel β-sheets stacked on top of each other—see Figure 1(a–c). To reduce the computational cost of our simulations, we retain only six neighboring peptides of 3OW9 which we immerse in 4317 water molecules. Six Cl^{-1} ions are also added to the simulation box to maintain the system neutral. This system is relaxed for 2.0 ns at 310 K and 1 atm.

To study dissociation, we used a two step Umbrella Sampling protocol.[43] In the first step, heavy atoms of five peptides of the preformed fibril were restrained to their initial positions using springs while the sixth peptide was pulled away along the x direction (see Fig. 1) in the NVT ensemble

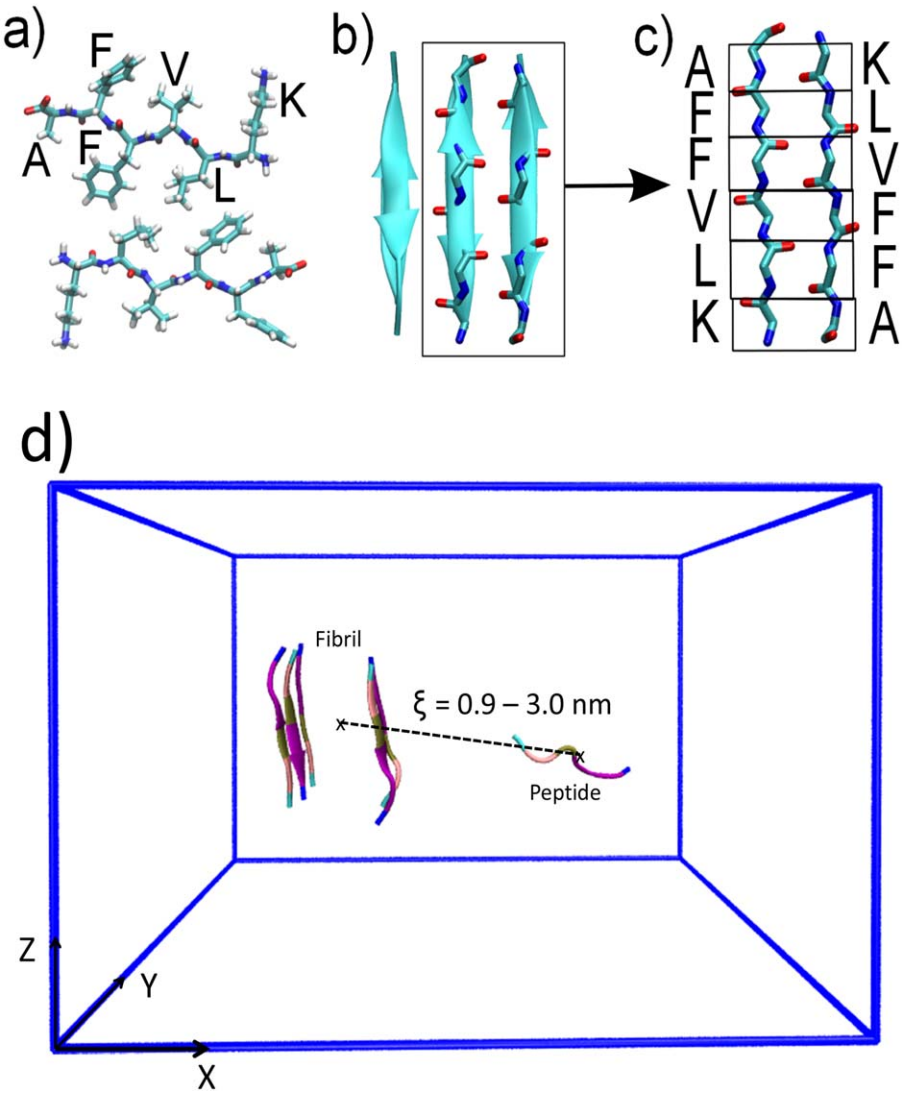

Figure 1

(Panels a–c) Fibril structure of Aβ_{16-21} (PDB ID: 3OW9). (**a**) Stacking of Aβ_{16-21} peptides. The peptide being pulled away is shown together with the one letter code of its amino acids. (**b**) Cartoon-like representation of the fibril. (**c**) Backbone structure of the peptide being pulled away (right) and its neighbor. Residues K, V, F_{20} of the pulled peptide are hydrogen bonded to the fibril while residues L, F_{19}, A are not hydrogen bonded.[80] (Panel d) Schematic representation of the preformed fibril, peptide that is being pulled away, and reaction coordinate ξ. A color code for residues is used in which cyan, beige, green, purple, and blue stand for lysine (K), leucine (L), valine (V), phenylalanine (F), and alanine (A), respectively. [Color figure can be viewed in the online issue, which is available at wileyonlinelibrary.com.]

for 1 ns. This short simulation was used to produce 26 configurations in which ξ (the distance between centers-of-mass of fibril and peptide) varied from 0.9 to 3.0 nm. Second, 26 molecular dynamics trajectories spanning 150 ns each were generated starting from the configurations produced in the first step. In these simulations, ξ was restrained to its initial value by a spring with equilibrium constant 1500 kJ mol^{-1} nm^2. The first 10 ns of these 26 trajectories was ignored and the last 140 ns was used to compute the potential of mean force (PMF) using the weighted histogram analysis method.[45] Thus, each PMF was computed from an accumulated time of 3.6 μs. This long simulation was required to produce repeat movements along the space spanned by ξ. Moreover, PMF(s) are computed at nine different temperatures accounting for an accumulated simulation time of 32 μs.

Simulations were conducted using the OPLS/AA force field and the TIP4P water model. A cut-off of 1.4 nm was used to account for short-range non-bonded interactions and long-range electrostatics were calculated using the Particle Mesh Ewald (PME) algorithm. An NPT ensemble was used in these simulations where temperature was controlled using the Nose-Hoover thermostat and pressure was fixed using the Parinello-Rahman barostat at 1 bar. To

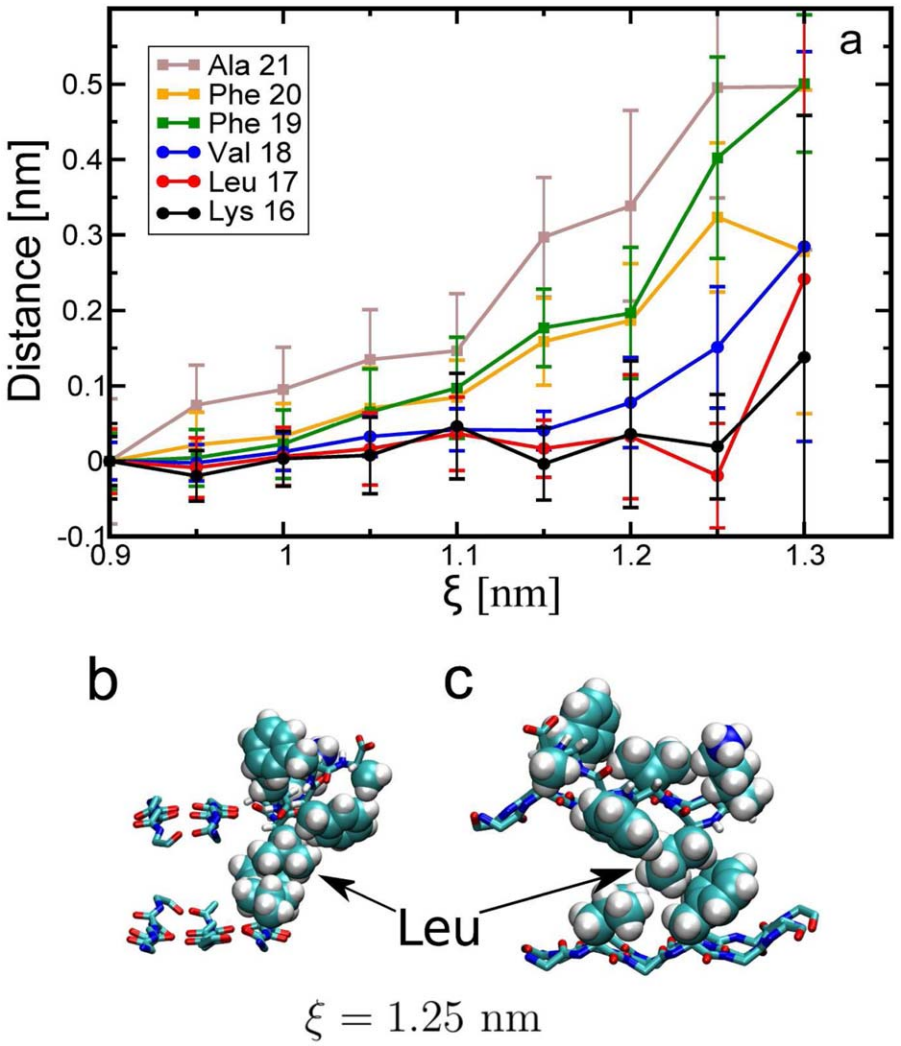

Figure 2

(**a**) Average distance between centers-of-mass of different residues of the peptide and the preformed fibril as a function of ξ. Error bars correspond to the root-mean-square-deviation of the distance in every window. The average distance at ξ=0.9 nm is used as our reference. Top (**b**) and side (**c**) views of the fibril before dissociation, that is, at ξ=1.25 nm. A van der Waals representation of selected side chains is shown. The backbone of all peptides is shown where red, blue and green colors are used to represent oxygen, nitrogen, and carbon atoms.

define hydrogen bonds we use a commonly used geometrical definition in which these bonds are formed when the distance between hydrogen (H) donor (D) and acceptor (A) is smaller than 0.4 nm and the angle H-D-A is smaller than 30°.

RESULTS

Peptide structure

To provide insights into the molecular interactions that are being ruptured during dissociation of $A\beta_{16-21}$, we show in Figure 2 average distances between centers-of-mass of residues in the pulling peptide and the preformed fibril at different ξ and for $\xi \leq 1.3$ nm, that is, before rupture. It is clear from panel a in this figure that the C-terminal (the last three residues: $F_{19}F_{20}A$) dissociates before the N-terminal (the first three residues: KLV). At ξ=1.25 nm, only leucine and lysine remain attached to the fibril while the other residues have moved at least 0.1 nm away from the fibril. At ξ=1.3 nm all the residues have moved more than 0.1 nm away from the fibril. The structure of the most representative cluster at ξ=1.25 nm is shown in Figure 2(b,c). In this structure, leucine of the peptide being pulled away is deeply embedded in the hydrophobic pocket of the fibril (formed by leucine and phenylalanine, that is, residue 19, of the peptide facing it). Surprisingly, this leucine residue is not hydrogen bonded

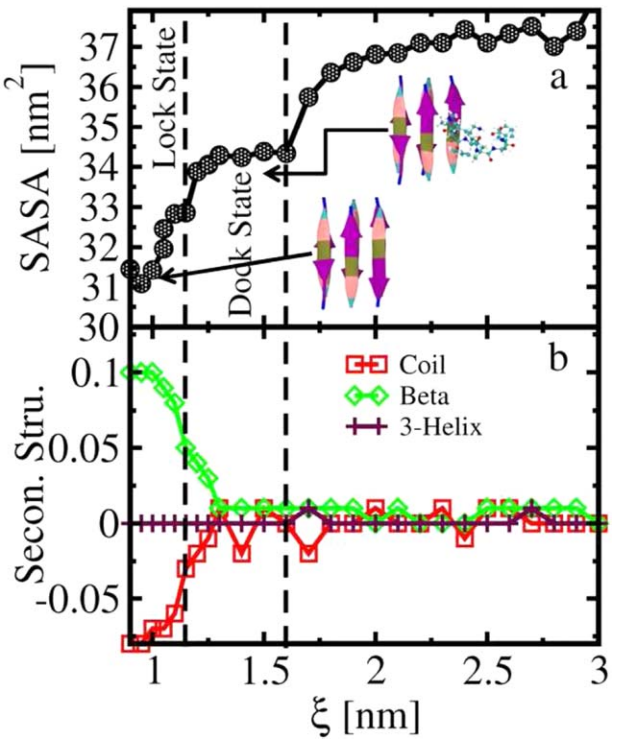

Figure 3

(**a**) Dependence of the solvent accessible surface area (SASA) on ξ which is used to define dock and lock states. (**b**) Fractions of coil, beta-structures, and 3-helix. Quantities computed at ξ=3.0 nm are used as our reference. [Color figure can be viewed in the online issue, which is available at wileyonlinelibrary.com.]

to the fibril which indicates that its stability is determined mainly by hydrophobic and van der Waals interactions.

In Figure 3(a) we show the solvent accessible surface area (SASA) as a function of ξ. SASA increases as Aβ_{16-21} dissociates from the fibril, exhibiting a plateau at intermediate distances (1.15 nm $<\xi<$ 1.6 nm). A sample conformation at one of these intermediate ξ values is shown indicating that the peptide forms van der Waals contacts with native chains in the fibril but it does not have the proper alignment required for hydrogen bonding. Conformations with ξ values within the plateau region of SASA are defined as dock states. SASA assumes its lowest value at the global minimum of the PMF, that is, in the lock state. In Figure 3(b) we study fractions of coil, β-structures, and 3-helix computed using DSSP[46] at different ξ values compared to ξ=3.0 nm. For example, since 66% and 55% of the residues form β-structures at ξ=0.9 nm and 3.0 nm, respectively, the fraction of β-structures in the lock state is ~0.11. In the lock state, the Aβ_{16-21} peptide forms mostly β structures while in dock and monomeric states it assumes mostly coil structures. The transition between these two states is abrupt.

Thermodynamics

In Figure 4(a) we show PMF(s) to dissociate an Aβ_{16-21} peptide from a preformed fibril at 283, 298, 310, 330, 345, 360, 370, 380, and 400K. PMF(s) are measured in kJ/mol and they are computed as described in the methodology section. Vertical dashed lines in Figure 4 separate ξ values for which the peptide is locked ($\xi<1.15$ nm), docked (1.15 nm $<\xi<1.6$ nm), and dissociated ($\xi>1.6$ nm) from the fibril as defined by the solvent accessible surface area in Figure 3. PMF(s) are characterized by a global minimum at ξ=0.9 nm that corresponds to lock states and they describe a downhill process in which no energetic barrier separates lock and monomeric states. The temperature dependence of the PMF obeys the thermodynamic relation[8,11,47]:

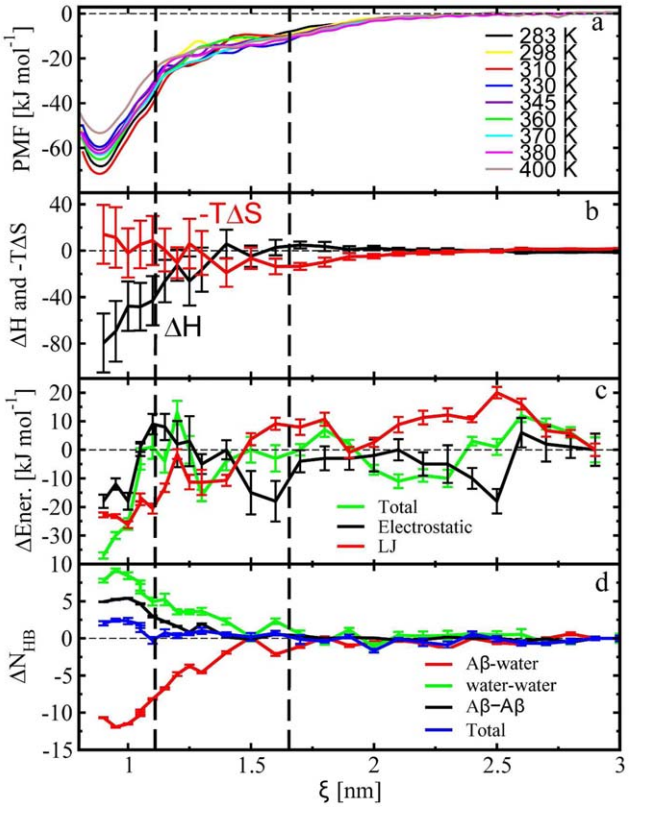

Figure 4

(**a**) PMF(s) to dissociate an Aβ_{16-21} peptide from a preformed fibril as a function of ξ at different temperatures. (**b**) Enthalpic (ΔH) and entropic ($-T\Delta S$) contributions to the PMF as a function of ξ at 310 K. Error bars were estimated based on the fit of the PMF to Eq. (1). (**c**) Electrostatic, Lennard-Jones (LJ), and their sum (total) as a function of ξ. (**d**) Changes in the number of hydrogen bonds as a function of ξ. Aβ–Aβ, Aβ–water, and water–water refer to hydrogen bonds between peptide-peptide, peptide-water, and water-water atoms. Error bars in panels c and d were computed from block averages where the trajectory was divided in five blocks. Quantities computed at ξ=3.0 nm are used as our reference. [Color figure can be viewed in the online issue, which is available at wileyonlinelibrary.com.]

$$\mathrm{PMF}(\xi, T) = \Delta H(\xi, T_o) - T\Delta S(\xi, T_o) + \Delta C_p(\xi, T_o)\left[(T - T_o) - T\log\left(\frac{T}{T_o}\right)\right], \quad (1)$$

where $\Delta H(\xi, T_o)$, $\Delta S(\xi, T_o)$, and $\Delta C_p(\xi, T_o)$ correspond to changes in the enthalpy, entropy, and heat capacity at T_o. To provide insight into how ΔH and $-T_o\Delta S$ contribute to the PMF at $T_o = 310$K, we fit our PMF(s) to Eq. (1) for each ξ value.[48,49] ΔH and $-T\Delta S$ are illustrated in Figure 4(b) showing that the PMF is dominated by enthalpy while dissociation accounts for only a small change in the entropic energy. $-T\Delta S$ is expected to emerge mainly from differences in the number of conformations of the peptide (configurational entropy) and water molecules around the peptide (shell water) that contribute favorably and unfavorably, respectively, to dissociation.[39] The number of conformations that a peptide can assume increases drastically with its size.[50] For small peptides, for example, Aβ_{16-21}, the increase in the configurational entropy during dissociation could be compensated by the entropic cost of solvating non-polar side accounting for the observed small $-T\Delta S$.

Notice that the fit of the computed PMF(s) to Eq. (1) also provide an estimate of $\Delta C_p(\xi, T_o)$.[51] This quantity is associated to the curvature of the PMF with respect to temperature [see Eq. (1)]. This requires accurate estimates of the PMF and large errors are often associated with ΔC_p computed from molecular dynamics simulations. Accordingly, from our least-square-fit we find that at ξ=0.95 nm and $T_o = 310$ K, $\Delta C_p = 0.31 \pm 0.82$ kJ mol^{-1} K^{-1}. While we can conclude from this estimate that ΔC_p is small, it is not possible to infer its sign with confidence. Determining the sign of ΔC_p could be a means to quantify the role played by non-polar groups in the stability of fibrils. For example, in the case of globular proteins ΔC_p of unfolding is positive and its magnitude increases with the number of non-polar residues that become exposed to the solvent.[12,52] This has been an important argument in favor of the hydrophobic effect being a main interaction stabilizing native protein structures[53] although rupture of intra-backbone hydrogen bonds has also been associated to the large and positive ΔC_p of protein unfolding.[54] In the case of fibril, both non-polar side chains and polar groups of the backbone could contribute significantly to ΔC_p of peptide dissociation. Since a positive and negative change in heat capacity are ascribed to non-polar and polar solvation,[52,55] ΔC_p for peptide dissociation could be both positive and negative. Accordingly, ΔC_p for fibrillization of insulin has been reported to be negative,[56] whereas it was found to be positive for the N47A mutant of the α-spectrin SH3 domain.[18] More extensive simulations are required to decrease error bars in our computed ΔC_p.

In Figure 4(c) we study how electrostatic and Lennard–Jones components of the enthalpy contribute to adding Aβ_{16-21} to the fibril. The electrostatic energy increases in the dock state and it decreases in the lock state as Aβ_{16-21} approaches the fibril. The latter can be explained by electrostatic interactions between peptide-water and fibril-water that are lost as ξ decreases without being compensated by favorable peptide-fibril electrostatic energy [see Fig. 5(a)]. In contrast, the reduction in electrostatic energy as the peptide locks into the fibril is dominated by favorable electrostatic interactions between peptide–fibril and water–water [see Fig. 5(a)]. In Figure 4(c) we observe that the Lennard–Jones energy decreases almost continuously in dock and lock states as ξ decreases. It is dominated by the formation of Lennard–Jones interactions between peptide-fibril [see Fig. 5(b)]. The sum of electrostatic and Lennard–Jones energies [see Fig. 4(c)] fluctuates considerably around zero in the dock and dissociated states whereas it decreases in the lock state with decreasing ξ.

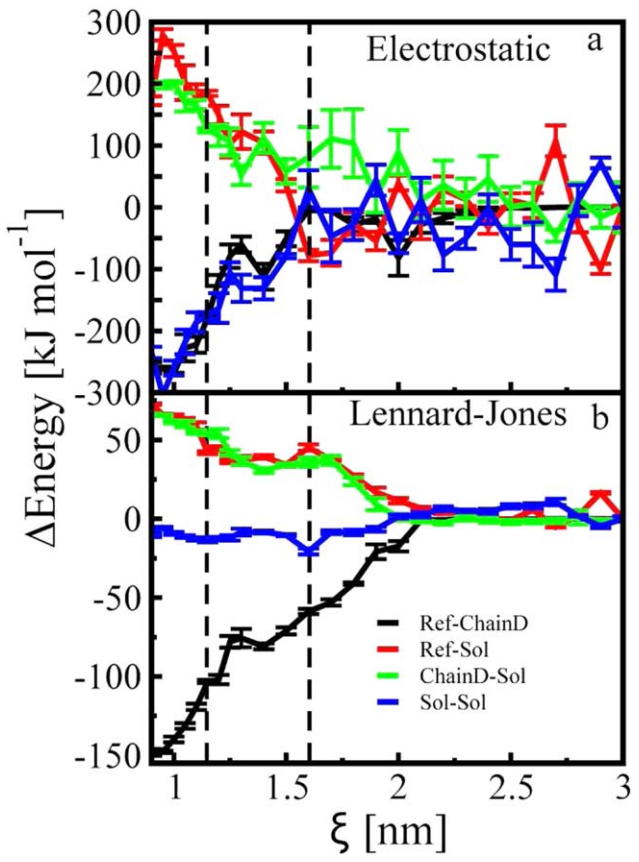

Figure 5

(**a**) Electrostatic and (**b**) Lennard–Jones energies decomposed into peptide–fibril (black), peptide–water (red), fibril–water (green), and water–water (blue) interactions. Pep–fib, pep–wat, fib–wat, and wat–wat refer to projections of the energy into peptide-fibril, peptide-water, fibril-water and water-water interactions. Error bars were computed through block averages where the trajectory was divided in five blocks. Quantities computed at ξ=3.0 nm are used as our reference. [Color figure can be viewed in the online issue, which is available at wileyonlinelibrary.com.]

In Figure 4(d), we study how the number of hydrogen bonds changes as a function of ξ. As shown previously[57–59] there is a compensatory mechanism in which the formation of one interpeptide hydrogen bond is preceded by the rupture of two peptide–water bonds leading to the formation of one additional water–water bond. For the dissociation process studied here, the compensation is not perfect as there are 2.5 additional hydrogen bonds in the system when the peptide is locked into the fibril compared to when it is in solution. Since in all-atom models, hydrogen bonds emerge from electrostatic interactions involving two electronegative atoms and one hydrogen, the formation of 2.5 extra hydrogen bonds in the lock state could explain part of the favorable electrostatic energy at $\xi \sim 0.9$ in Figure 4(c).

Volumetric properties

In Figure 6(a), we show the effective volume change of the system $\Delta V(\xi)$ when the peptide is brought to a distance ξ from the fibril all the way from ξ=3.0 nm at 310 K. In other words, $\Delta V(\xi) \equiv V(\xi) - V(3.0\ \text{nm})$, where $V(\xi)$ is the average volume of the simulation box at ξ. Notice that the volume occupied by water molecules that are at a large distance from the fibril/peptide, that is, bulk water, does not depend on ξ. Therefore, bulk water does not contribute to $\Delta V(\xi)$. Only the volume of molecules around the peptide will contribute to $\Delta V(\xi)$. The maximum volume change occurs when the peptide dissociates from the lock state (ξ=0.9 nm) and its magnitude is $\sim$0.05 nm^3. This corresponds approximately to the volume of one water molecule at ambient conditions.[48] This ΔV is consistent with the volume change to dissociate a disulfide deficient variant of hen lysozyme from a fibril which was reported to be 0.0166 nm^3 (that is, 52.7 mL/mol per monomeric unit).[60] In contrast, insulin was reported to pack efficiently in the fibrillar state as to decrease the overall volume by 3%.[61]

At fixed ξ value, $\Delta V(\xi)$ decreases with increasing temperature [see Figure 6(a)]. To quantify this effect of temperature on $\Delta V(\xi)$, we show $\frac{\partial \Delta V(\xi)}{\partial T}$ in Figure 6(b). This quantity was computed by fitting the temperature dependence of $\Delta V(\xi)$ to:

$$\Delta V(\xi) = \Delta V_o + \left(\frac{\partial \Delta V(\xi)}{\partial T}\right)\Big|_{T_o} (T - T_o), \qquad (2)$$

where we used $T_o = 310$ K. Notice that $\frac{\partial \Delta V(\xi)}{\partial T}$ is proportional to the thermal expansion coefficient of peptide addition to the fibril. It is negative for all ξ values and it tends to zero continuously as shown in Figure 6(b).

As a comparison, the volume change associated with protein folding ΔV^* is also small, for example, $\sim$90 ml/mol for SNase[62–64] which is the equivalent of $\sim$0.14 nm^3 per protein molecule. It has a positive sign that is attributed to packing defects in the folded state.[65] The

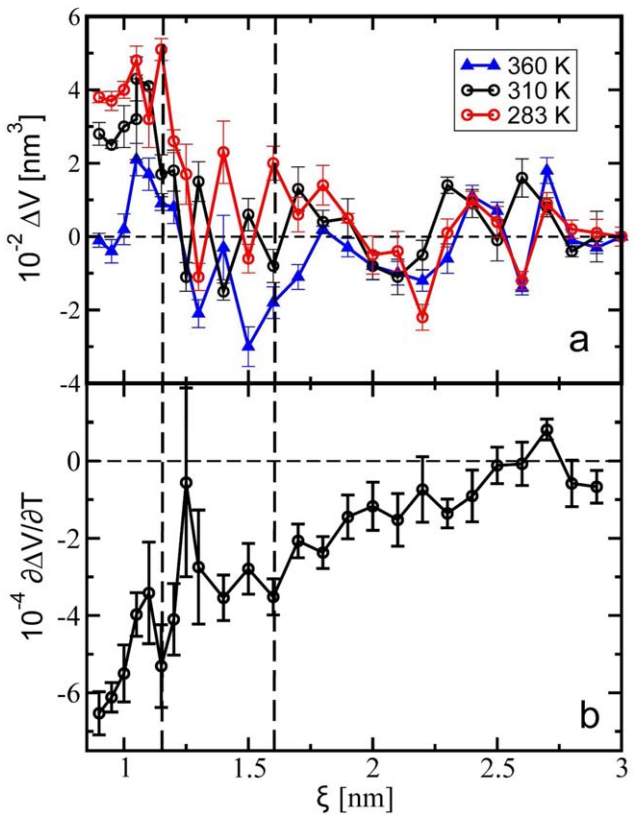

Figure 6

(**a**) Average volume of the simulation box as a function of ξ at 283, 310, and 360 K. The average volume computed at ξ=3.0 nm is used as our reference. Error bars correspond to the root-mean-square deviation of the volume at ξ. (**b**) Derivative of the association volume of Aβ_{16-21} into a fibril as a function of temperature computed at 310 K. Error bars were computed from estimated errors in the least square fit given by Eq. (2). [Color figure can be viewed in the online issue, which is available at wileyonlinelibrary.com.]

later accounts for empty spaces otherwise not present in the unfolded protein as water molecules can occupy any interstitial due to its small size.[66,67] Thus, unfolding minimizes the volume of the system through the annihilation of empty space. Furthermore, for protein folding ΔV^* decreases with increasing temperature[68] which accounts for a negative thermal expansion coefficient of folding $\Delta\alpha^*$.[68] Thus, with respect to the volume change and the sign of the thermal expansion coefficient, protein folding and peptide addition to a fibril share common features. This is consistent with the reported fibrillization of insulin that accounted for reduction in the thermal expansion coefficient of about 30%.[61]

According to Le Chatelier's principle increasing the applied pressure on a system favors states that occupy small volumes. Thus, an implication of the positive ΔV^* for protein folding is that increasing pressure favors unfolding.[48,64,67,69–72] Similarly, the computed positive ΔV for peptide addition suggests that increasing pressure favors the dissociated state with respect to the fibrillar

state. This could be the rational for experiments in which applied pressure caused amyloid fibril dissociation.[73–76] Recently, the basis of how ΔV affects the free-energy associated with conformational changes in proteins has been investigated using computer simulations.[48,57,77] It was reported that ΔV in the assembly of restrained α-helices correlates with the enthalpy of the system,[77] and in the interactions between extended peptides it correlates with the electrostatic energy of system.[57] Despite these results, the relation between volume change and energy could be more complex for nonrestrain systems. Accordingly, no clear correlation is observed here between ΔV of dissociation [Fig. 6(a)] and ΔH [Fig. 4(b)].

CONCLUSION

In summary, thermodynamic quantities describing peptide dissociation from a fibril are not easily accessible experimentally but insights can be obtained from computer simulations. Here, we provided insights into these quantities and their molecular basis by computing PMF(s) to remove an Aβ_{16-21} peptide from a preformed fibril at different temperatures using all-atom molecular dynamics simulations in explicit water. We used the distance ξ between centers-of-mass of the Aβ_{16-21} peptide and the preformed fibril as the reaction coordinate. The temperature dependence of the PMF was used to determine changes in the enthalpy and entropy during dissociation while the average volume of the simulation box was computed as a function of ξ. We found that the PMF is dominated by enthalpy while the entropic energy does not change significantly during dissociation. In systems where the loss of configurational entropy competes with attractive molecular interactions, for example, during binding of actin filament, the free-energy landscape of binding-unbinding transitions can exhibit an energy barrier that accounts for a discontinuous transition.[78] This is not the case in our system where the PMF for peptide dissociation characterizes a downhill process without an energy barrier.

The computed heat capacity of dissociation in our simulations, which determines the curvature of the PMF with respect to temperature, was found to be small. More extensive computer simulations are needed to provide a confident estimate of its sign which could be valuable in determining the role played by the hydrophobic effect in fibril stability.[19,79] The volume of the simulation box was found to decrease during dissociation. Moreover, the magnitude of this volume change with respect to temperature was found to decrease with increasing temperature.

These results can be cast in light of the thermodynamics of protein unfolding which is well established. During unfolding of globular proteins both the enthalpy and the entropic energy change significantly compensating each other and accounting for a small change in the free-energy. This enthalpy-entropy compensation was not observed in our simulations of peptide dissociation as the entropy did not change significantly. The latter could be related to the small size of Aβ_{16-21}. Also, the change in heat capacity which is large for protein unfolding was found to be negligible for peptide dissociation. This suggests that non-polar groups of Aβ_{16-21}, that is, carboxyl and amine groups of the backbone, could contribute significantly in determining ΔC_p. Despite these differences, the main term contributing to the free-energy of unfolding and the computed PMF(s) for peptide dissociation is enthalpy at 310 K. With respect to the change in volume both unfolding and dissociation account for a reduction in the volume of the system. Moreover, the magnitude of the latter in our simulations decreases with increasing temperature implying that the thermal expansion coefficient for peptide dissociation (addition) is positive (negative). Experimentally, the sign of the thermal expansion coefficient of unfolding (folding) was measured to be positive (negative)[68–70] suggesting that a same molecular mechanism, that is, annihilation of cavities during unfolding and peptide dissociation, could underlie volumetric properties in protein unfolding and peptide dissociation.

Our simulations show that the C-terminal of the pulled peptide dissociates first and leucine is the last residue to remain attached to the fibril. Leucine is not hydrogen bonded to the fibril but it is deeply buried its hydrophobic pocket. This highlights the importance of side-chain interactions in the stability of fibrils. Furthermore, our simulations show energetic differences between lock and dock states. In particular, the electrostatic energy of the system increases and decreases as the peptide dissociates in lock and dock states, respectively.

Despite these important insights into the thermodynamics of fibrils brought up by our accumulated 32 μs simulations, limitations of the current work should also be highlighted. In particular, more extensive simulations could be useful to decrease error bars and provide an estimate of the sign of the heat capacity of dissociation. Moreover, insights provided by our work into how enthalpy and entropy contribute to the dissociation free-energy could benefit from a comparison between different force-fields. This is, however, beyond the scope of the current work.

ACKNOWLEDGMENT

This work was made possible by NJIT start-up funds and computational resources available through Compute Canada.

REFERENCES

1. Dobson CM. Protein folding and misfolding. Nature 2003;426:884.
2. Hardy J, Higgins G. Alzheimer's disease: the amyloid cascade hypothesis. Science 1992;256:184.

3. Karran E, Mercken M, Strooper BD. The amyloid cascade hypothesis for alzheimer's disease: an appraisal for the development of therapeutics. Nat Revs Drug Discov 2011;10:698–712.
4. Kushner AM, Guan Z. Modular design in natural and biomimetic soft materials. Angew Chem Int Ed 2011;50:9026.
5. Nova A, Keten S, Pugno NM, Redaelli A, Buehler MJ. Molecular and nanostructural mechanisms of deformation, strength and toughness of spider silk fibrils. Nano Lett 2010;10:2626–2634.
6. Chiti F, Dobson CM. Protein misfolding, functional amyloid, and human disease. Annu Rev Biochem 2006;75:333.
7. Hamley I. The amyloid beta peptide: a chemist's perspective. role in alzheimer's and fibrillization. Chem Rev 2012;112:5147–5192.
8. Smeller L. Pressure-temperature phase diagrams of biomolecules. Biochim Biophys Acta (BBA) 2002;1595:11–29.
9. Privalov PL. Thermodynamics of protein folding. J Chem Thermodyn 1997;29:447.
10. Robertson AD, Murphy KP. Protein structure and the energetics of protein stability. Chem Rev 1997;97:1251
11. Dias CL, Ala-Nissila T, Wong-ekkabut J, Vattulainen I, Grant M, Karttunen M. The hydrophobic effect and its role in cold denaturation. Cryobiology 2010;60:91–99.
12. Myers JK, Nick Pace C, Martin Scholtz J. Denaturant m values and heat capacity changes: relation to changes in accessible surface areas of protein unfolding. Protein Sci 1995;4:2138–2148.
13. Kauzmann W. Some factors in the interpretation of protein denaturation. Adv Protein Chem 1959;14:1–63.
14. Frank HS, Evans MW. Free volume and entropy in condensed systems iii. entropy in binary liquid mixtures; partial molal entropy in dilute solutions; structure and thermodynamics in aqueous electrolytes. J Chem Phys 1945;13:507.
15. Sharp K. Entropy-enthalpy compensation: fact or artifact? Protein Sci 2001;10:661–667.
16. Doyle CM, Rumfeldt JA, Broom HR, Broom A, Stathopulos PB, Vassall KA, Almey JJ, Meiering EM. Energetics of oligomeric protein folding and association. Arch Biochem Biophys 2013;531:44–64.
17. Kardos J, Yamamoto K, Hasegawa K, Naiki H, Goto Y. Direct measurement of the thermodynamic parameters of amyloid formation by isothermal titration calorimetry. J Biol Chem 2004;279:55308–55314.
18. Morel B, Varela L, Conejero-Lara F. The thermodynamic stability of amyloid fibrils studied by differential scanning calorimetry. J Phys Chem B 2010;114:4010–4019.
19. Ikenoue T, Lee YH, Kardos J, Saiki M, Yagi H, Kawata Y, Goto Y. Cold denaturation of alpha-synuclein amyloid fibrils. Angew Chem Int Ed 2014;53:7799–7804.
20. Jeppesen MD, Hein K, Nissen P, Westh P, Otzen DE. A thermodynamic analysis of fibrillar polymorphism. Biophys Chem 2010;149:40–46.
21. Harper JD, Wong SS, Lieber CM, Lansbury PT. Observation of metastable aβ amyloid protofibrils by atomic force microscopy. Chem Biol 1997;4:119–125.
22. Invernizzi G, Papaleo E, Sabate R, Ventura S. Protein aggregation: Mechanisms and functional consequences. Int J Biochem Cell Biol 2012;44:1541–1554.
23. Uversky VN, Li J, Fink AL. Evidence for a partially folded intermediate in α-synuclein fibril formation. J Biol Chem 2001;276:10737.
24. Sabaté R, Gallardo M, Estelrich J. An autocatalytic reaction as a model for the kinetics of the aggregation of β-amyloid. Peptide Sci 2003;71:190–195.
25. Nguyen P, Derreumaux P. Understanding amyloid fibril nucleation and aβ oligomer/drug interactions from computer simulations. Acc Chem Res 2014;47:603.
26. Collins S, Douglass A, Vale R, Weissman J. Mechanism of prion propagation: amyloid growth occurs by monomer addition. PLoS Biol 2004;2:e321.
27. Cannon MJ, Williams AD, Wetzel R, Myszka DG. Kinetic analysis of beta-amyloid fibril elongation. Anal Biochem 2004;328:67–75.
28. Willemsen OH, Snel MME, Cambi A, Greve J, Grooth BGD, Figdor CG. Biomolecular interactions measured by atomic force microscopy. Biophys J 2000;79:3267.
29. Esler WP, Stimson ER, Jennings JM, Vinters HV, Ghilardi JR, Lee JP, Mantyh PW, Maggio JE. Alzheimer's disease amyloid propagation by a template-dependent dock-lock mechanism. Biochemistry 2000;39:6288–6295.
30. Gobbi M, Colombo L, Morbin M, Mazzoleni G, Accardo E, Vanoni M, Del Favero E, Cantù L, Kirschner DA, Manzoni C, Beeg M, Ceci P, Ubezio P, Forloni G, Tagliavini F, Salmona M. Gerstmann-sträussler-scheinker disease amyloid protein polymerizes according to the" dock-and-lock" model. J Biol Chem 2006;281:843–849.
31. Schor M, Vreede J, Bolhuis PG. Elucidating the locking mechanism of peptides onto growing amyloid fibrils through transition path sampling. Biophys J 2012;103:1296–1304.
32. Buchete NV. Unlocking the atomic-level details of amyloid fibril growth through advanced biomolecular simulations. Biophys J 2012;103:1411.
33. Han M, Hansmann UH. Replica exchange molecular dynamics of the thermodynamics of fibril growth of alzheimer's aβ42 peptide. J Chem Phys 2011;135:065101.
34. Takeda T, Klimov DK. Dissociation of aβ_{16-22} amyloid fibrils probed by molecular dynamics. J Mol Biol 2007;368:1202.
35. Takeda T, Klimov DK. Replica exchange simulations of the thermodynamics of aβ fibril growth. Biophys J 2009;96:442
36. Reddy G, Straub JE, Thirumalai D. Dynamics of locking of peptides onto growing amyloid fibrils. Proc Natl Acad Sci USA 2009;106:11948.
37. Krone MG, Hua L, Soto P, Zhou R, Berne BJ, Shea JE. Role of water in mediating the assembly of alzheimer amyloid-β aβ16-22 protofilaments. J Am Chem Soc 2008;130:11066–11072.
38. Reddy G, Straub JE, Thirumalai D. Dry amyloid fibril assembly in a yeast prion peptide is mediated by long-lived structures containing water wires. Proc Natl Acad Sci 2010;107:21459–21464.
39. Thirumalai D, Reddy G, Straub JE. Role of water in protein aggregation and amyloid polymorphism. Acc Chem Res 2012;45:83.
40. Wetzel R. Kinetics and thermodynamics of amyloid fibril assembly. Acc Chem Res 2006;39:671–679.
41. O'Nuallain B, Shivaprasad S, Kheterpal I, Wetzel R. Thermodynamics of a$_\beta$(1-40) amyloid fibril elongation. Biochemistry 2005;44:12709.
42. Williams AD, Shivaprasad S, Wetzel R. Alanine scanning mutagenesis of aβ(1-40) amyloid fibril stability. J Mol Biol 2006;357:1283 –1294.
43. Lemkul JA, Bevan DR. Assessing the stability of alzheimer's amyloid protofibrils using molecular dynamics. J Phys Chem B 2010;114:1652
44. Colletier J, Laganowsky A, Landau M, Zhao M, Soriaga A, Goldschmidt L, Flot D, Cascio D, Sawaya MR, Eisenberg D. Molecular basis for amyloid-β polymorphism. Proc Natl Acad Sci USA 2011;108:16938.
45. Hub JS, de Groot BL, van der Spoel D. g_wham—a free weighted histogram analysis implementation including robust error and autocorrelation estimates. J Chem Theory Comput 2010;6:3713
46. Kabsch W, Sander C. Dictionary of protein secondary structure: pattern recognition of hydrogen-bonded and geometrical features. Biopolymers 1983;22:2577.
47. Kunugi S, Tanaka N. Cold denaturation of proteins under high pressure. Biochim Biophys Acta 2002;1595:329–344.
48. Dias CL, Chan HS. Pressure-dependence properties of elementary hydrophobic interactions: Ramifications for activation properties of protein folding. J Phys Chem B 2014;118:7488–7509.
49. Shimizu, S, Chan, HS. Temperature dependence of hydrophobic interactions: a mean force perspective, effects of water density, and nonadditivity of thermodynamic signatures. J Chem Phys 2000;113:4683
50. Machta J, Kirkpatrick T. Self-avoiding walks and manifolds in random environments. Phys Rev A 1990;41:5345
51. Simizu S, Chan HS. Configuration-dependent heat capacity of pairwise hydrophobic interactions. J Am Chem Soc 2001;123:2083

52. Prabhu NV, Sharp KA. Heat capacity in proteins. Annu Rev Phys Chem 2005;56:521
53. Dill KA. Dominant forces in protein folding. Biochemistry 1990;29: 7133
54. Cooper A. Heat capacity of hydrogen-bonded networks: an alternative view of protein folding thermodynamics. Biophys Chem 2000; 85:25
55. Edsall JT. Apparent molal heat capacities of amino acids and other organic compounds. J Am Chem Soc 1935;54:1506–1507.
56. Smirnovas V, Winter R. Revealing different aggregation pathways of amyloidogenic proteins by ultrasound velocimetry. Biophys J 2008; 94:3241
57. Narayanan C, Dias CL. Hydrophobic interactions and hydrogen bonds in β-sheet formation. J Chem Phys 2013;139:115103
58. Su Z, Dias CL. Driving β-strands into fibrils. J Phys Chem B 2014; 118:10830–10836.
59. Jorgensen WL. Interactions between amides in solution and the thermodynamics of weak binding. J Am Chem Soc 1989;111:3770
60. Niraula TN, Konno T, Li H, Yamada H, Akasaka K, Tachibana H. Pressure-dissociable reversible assembly of intrinsically denatured lysozyme is a precursor for amyloid fibrils. Proc Natl Acad Sci USA 2004;101:4089.
61. Smirnovas V, Winter R, Funck T, Dzwolak W. Protein amyloidogenesis in the context of volume fluctuations: a case study on insulin. ChemPhysChem 2006;7:1046–1049.
62. Brandts JF, Oliveira RJ, Westort C. Thermodynamics of protein denaturation. effect of pressure on the denaturation on ribonuclease A. Biochemistry 1970;9:1038
63. Chalikian TV. Volumetric properties of proteins. Annu Rev Biophys Biomol Struct 2003;32:207–235.
64. Royer CA. Revisiting volume changes in pressure-induced protein unfolding. Biochim Biophys Acta 2002;1595:201–209. March,.
65. Roche J, Caro JA, Norberto DR, Barthe P, Roumestand C, Schlessman JL, Garcia AE, Garca-Moreno BE, Royer CA, Cavities determine the pressure unfolding of proteins. Proc Natl Acad Sci USA 2012; 109:6945–6950.
66. Hummer G, Garde S, Garcia AE, Paulaitis ME. The pressure dependence of hydrophobic interactions is consistent with the observed pressure denaturation of proteins. Proc Natl Acad Sci USA 1998;95:1552
67. Dias CL. Unifying microscopic mechanism for pressure and cold denaturations of proteins. Phys Rev Lett 2012;109:048104–048109.
68. Panick G, Vidugiris GJA, Malessa R, Rapp G, Winter R, Royer CA. Exploring the temperature-pressure phase diagram of staphylococcal nuclease. Biochemistry 1999;38:4157–4164.
69. Zipp A, Kauzmann W. Pressure denaturation of metmyoglobin. Biochemistry 1973;12:4217 –4228.
70. Hawley SA. Reversible pressure-temperature denaturation of chymotrypsinogen. Biochemistry 1971;10:2436 –2442.
71. Seemann H, Winter R, Royer CA. Volume, expansivity and isothermal compressibility changes associated with temperature and pressure unfolding of staphylococcal nuclease. J Mol Biol 2001;307: 1091–1102.
72. Voloshin VP, Medvedev NN, Smolin N, Geiger A, Winter R. Exploring volume, compressibility and hydration changes of folded proteins upon compression. Phys Chem Chem Phys 2015;17:8499–8508.
73. Dirix C, Meersman F, MacPhee CE, Dobson CM, Heremans K. High hydrostatic pressure dissociates early aggregates of $ttr_{105-115}$, but not the mature amyloid fibrils. J Mol Biol 2005;347:903 –909.
74. El Moustaine D, Perrier V, Van Ba IAT, Meersman F, Ostapchenko VG, Baskakov IV, Lange R, Torrent J. Amyloid features and neuronal toxicity of mature prion fibrils are highly sensitive to high pressure. J Biol Chem 2011;286:13448–13459.
75. Winter R, Dzwolak W. Exploring the temperature-pressure configurational landscape of biomolecules: from lipid membranes to proteins. Philos Trans R Soc Math Phys Eng Sci 2005;363:537–563.
76. Dzwolak W, Ravindra R, Lendermann J, Winter R. Aggregation of bovine insulin probed by dsc/ppc calorimetry and ftir spectroscopy. Biochemistry 2003;42:11347
77. MacCallum JL, Sabaye Moghaddam M, Chan HC, Tieleman DP. Hydrophobic association of α-helices, steric dewetting and enthalpic barriers to protein folding. Proc Natl Acad Sci USA. 2007;104:6206
78. Kierfeld J, Kühne T, Lipowsky R. Discontinuous unbinding transitions of filament bundles. Phys Rev Lett 2005;95:038102
79. Mishra R, Winter R. Cold- and pressure-induced dissociation of protein aggregation and amyloid fibrils. Angew Chem Int Ed 2008; 47:6518
80. Urbic T, Dias C. Hydration of non-polar anti-parallel beta-sheets. J Chem Phys 2014;140:165101